Pflugers Arch - Eur J Physiol (2014) 466:2153–2165
DOI 10.1007/s00424-014-1443-0

SENSORY PHYSIOLOGY

Reduced excitability of gp130-deficient nociceptors is associated with increased voltage-gated potassium currents and Kcna4 channel upregulation

Michiel Langeslag · Philipp Malsch · Andrea Welling · Michaela Kress

Received: 8 November 2013 / Revised: 18 December 2013 / Accepted: 4 January 2014 / Published online: 25 January 2014

Abstract Neuropathic pain and pain arising from local inflammation are characterized by increased release of inflammatory mediators like interleukin-6 (IL-6) by immune cells. The levels of IL-6 is increased in various painfull conditions and correlates with the severity of thermal and mechanical hypersensitivity. Deletion of the IL-6 signal transducer glycoprotein 130 (gp130) reduces inflammation associated with hypersensitivity to thermal and mechanical stimuli. In this study, we show that nociceptor-specific deletion of gp130 alters excitability parameters that are linked to changes in the potassium conductance. In SNS-gp130$^{-/-}$ sensory neurons, the resting membrane potential was reduced. Moreover the repolarization speed of the action potential and afterhypolarization was augmented, however, voltage-gated Na^+ and Ca^{2+} current were not obviously altered. The main difference between gp130-deficient and control neurons was a significant increase in the conductance of both delayed rectifier as well as A-type potassium currents. Taqman RT-PCR analysis revealed significantly higher levels of *Kcna4* mRNA, encoding A-type Kv1.4 potassium channel, in neuron cultures from SNS-gp130$^{-/-}$ versus control mice, which may account for the electrophysiological data. No difference in other voltage-gated ion channel mRNAs was observed. The present data show for the first time increased A-type K^+ currents and expression of voltage-gated potassium channel *Kcna4* (Kv1.4) in SNS-gp130$^{-/-}$ nociceptors. This suggests that gp130 acts as a break for the expression of potassium channels and important regulator hub for nociceptor excitability.

Keywords Glycoprotein 130 · Nociceptor · Excitability · Voltage-gated K^+ channels

M. Langeslag (✉) · P. Malsch · M. Kress
Department of Physiology and Biomedical Physics, Division of Physiology, Medical University of Innsbruck, Fritz-Pregl Strasse 3-I, A-6020 Innsbruck, Austria
e-mail: michiel.langeslag@i-med.ac.at

A. Welling
Institute of Pharmacology und Toxicology, Technical University München, Biedersteiner Strasse 29, 80802 Munich, Germany

Introduction

Neuropathic pain and other persisting pain syndromes arise from aberrant excitability and ongoing activation of primary nociceptive afferents. Local inflammation at the injury site is characterized by invading immune cells and aberrant levels of inflammatory mediators like cytokines. Especially members of the interleukin-6 (IL-6) like family of cytokines are gaining increasing interest, since in chronic pain syndromes and painful inflammatory conditions like rheumatoid arthritis, the levels of IL-6 are greatly elevated, whereas under normal conditions, IL-6 is hardly detectable [6, 32, 38, 60]. Furthermore, IL-6 levels are increased following nerve injury and correlate well with development of thermal and mechanical hypersensitivity [20, 48]. IL-6 signals to target cells by binding to membrane-bound or soluble IL-6 receptor alpha subunits which heteromerize with the glycoprotein 130 (gp130) signal transducer [30, 31]. The majority of sensory neurons in the dorsal root ganglion express gp130 and specific subpopulations sense neuropoietic cytokines of the IL-6 family [7, 27]. The absence of gp130 from nociceptive primary afferents results in decreased IL-6 or Oncostatin M induced hypersensitivity to thermal stimuli [5, 43]. Besides, gp130 has a prominent role in the maintenance of mechanical hypersensitivity in experimental tumor, nerve injury or inflammation models of neuropathic pain [54].

Hypersensitivity to mechanical stimuli is potently induced by deregulation of mechanotransducer ion channels [46]. Voltage-dependent ion channels are key components in

signaling pathways downstream of these transduction cascades and may also be deregulated during an inflammatory process. Of these, voltage-gated sodium and calcium channels have intensely been studied in recent years [4, 12, 13, 28]. Surprisingly, the expression of voltage-gated potassium channels in nociceptors and their importance for nociceptor excitation and sensitisation has only recently started to gain broader interest, although they largely control neuronal excitability [37]. Specifically, axotomy of dorsal root ganglia (DRG) neurons decreases the expression of voltage-gated potassium channels and subsequently causes reduction of potassium currents to increase hyperexcitability [23, 34, 66].

Here, we set out to characterize the excitability of DRG neurons from nociceptor-specific gp130 knock-out (SNS-gp130$^{-/-}$) and control gp130 floxed (gp130$^{fl/fl}$) mice. A special emphasis was placed on the investigation of the action potential (AP) characteristics, and the biophysical properties of voltage-gated sodium, potassium, and calcium channels. Whereas no differences for sodium and calcium signatures were observed between gp130$^{fl/fl}$ and SNS-gp130$^{-/-}$ neurons, converging evidence was collected suggesting that potassium conductances were significantly upregulated. This resulted in a reduced excitability of SNS-gp130$^{-/-}$ nociceptive neurons accompanied by a faster repolarization phase of the AP. Taqman real-time polymerase chain reaction (RT-PCR) revealed increased expression of the voltage-gated, A-type K^+ channel Kv1.4 in SNS-gp130$^{-/-}$ nociceptors. This suggests that gp130 performs its role as a regulator of nociceptor excitability by inhibiting the expression of A-type potassium channels.

Materials and methods

Genetically modified mice

SNS-gp130$^{-/-}$ and gp130$^{fl/fl}$ mice were generated, bred, and genotyped as described previously [5]. All mice were maintained under specific pathogen-free (SPF) conditions. Littermates were used in all experiments to control for background effects. For all experiments, a statistically weighted number of animals was used. All animal use procedures were in accordance with ethical guidelines and animal welfare standards according to Austrian law.

Primary sensory neuron culture

Lumbar DRG containing the cell bodies of primary afferents that project into the hindpaw were harvested from adult mice (age 8–16 weeks) as previously published [5, 43]. After removal of the connective tissue, ganglia were incubated in Liberase Blendzyme 1 (9 mg/100 ml DMEM, Roche) for two times 30 min. After washing with phosphate buffered saline PBS (PAA), 1× Trypsin-EDTA (Invitrogen) was added for 15 min and DRG were washed with TNB™ medium (Biochrom) supplemented with L-glutamin (Invitrogen), penicillin G sodium, streptomycin sulfate (Invitrogen), and Protein-Lipid-Komplex™ (Biochrom). The DRG were dissociated with a fire-polished Pasteur pipette and centrifuged through a 3.5 % BSA gradient (Sigma) to eliminate non-neuronal cells. The sensory neurons were resuspended, plated on coverslips coated with poly-L-lysine/laminin-1 (Sigma), and cultivated in supplemented TNB™ containing mNGF 2.5S (Alomone Labs, 10 μg/100 ml TNB medium) at 37 °C in 5 % CO_2 for 24–36 h.

Live-cell labeling

Overnight, DRG neuron cultures were live cell labeled for gp130 shortly before recording. Cultures were incubated at RT with primary antibody against gp130 (Neuromics) diluted 1:50 in TNB™ medium for 45 min, washed with TNB™ medium for 10 min, and incubated with a AlexaFluor-488 conjugated secondary antibody (Invitrogen) diluted in TNB™ medium (1:500) for 30 min. Subsequently, cells were washed twice with TNB medium.

Patch-clamp recordings

DRG neurons in culture were used for electrophysiology 18 to 28 h after plating. In short, glass coverslips were mounted in a recording chamber and placed on a Zeiss Axiovert 200 microscope. Neurons were identified by the presence (gp130-positive) or absence (gp130-negative) of AlexaFluor-488 fluorescence. Ionic currents were recorded from isolated neurons in the whole-cell voltage-clamp configuration of the patch-clamp technique as previously published [5, 16, 50]. Only DRG neurons smaller than <35 μm were selected, representing the small to medium-sized neurons. Borosilicate glass pipettes (Science Products) were pulled with a horizontal puller (Sutter Instruments) and filled with internal solution (ICS, Table 1). Neurons were kept in a hydroxyethyl piperazineethanesulfonic acid (HEPES)-buffered extracellular solution (ECS, Table 2) and maintained at -80 mV holding potential. All measurements were recorded with an EPC 9 (HEKA) and the Pulse v8.74 software (HEKA). Experiments were performed at room temperature, and only one neuron was tested per Petri dish. Currents were sampled at 20 kHz for Na^+, K^+, and Ca^{2+} recordings and filtered at 2.9 kHz. Cellular voltage recordings were performed in whole-cell current-clamp mode of the patch clamp technique. Neurons were held at 0 pA, and voltage changes were sampled at 5 kHz and

Table 1 Intracellular solutions used for general excitability and specific ionic conductance

	KGlu	KCl	TEACl	NaCl	CsMeS	CsCl	$CaCl_2$	$MgCl_2$	EGTA	HEPES	Mg ATP	Na GTP	Sucrose
I_{all}	98	45	–	–	–	–	0.5	2	5	10	2	0.2	–
I_{Na^+}	–	–	–	10	138	–	0.1	2	1	10	2	–	–
I_{K^+}	–	148	–	–	–	–	0.5	2	5	10	2	0.2	–
$I_{Ca^{2+}}$	–	–	20	–	–	120	–	–	10	10	2	–	20

KGlu potassium D-gluconate, *TEACl* tetraethylammonium chloride, *CsMeS* cesium methanesulfonate

Concentrations are given in mM, pH of all external solutions were set to 7.3 with KOH (I and I_{K^+}) or CsOH (I_{Na^+} and $I_{Ca^{2+}}$)

filtered at 2.9 kHz. Tetrodotoxin (TTX, final concentration 250 nM) and 4-AP at a final concentration of 5 mM (both Sigma-Aldrich) were added by bath application to the recorded cells, and the maximal inhibition was monitored in voltage-clamp configuration by applying a depolarizing block pulse protocol to -10 mV for 25 ms from the holding potential.

Analysis

Action potentials

In order to assess the passive membrane properties, the input resistance of $gp130^{fl/fl}$ and SNS-$gp130^{-/-}$ DRG neurons was

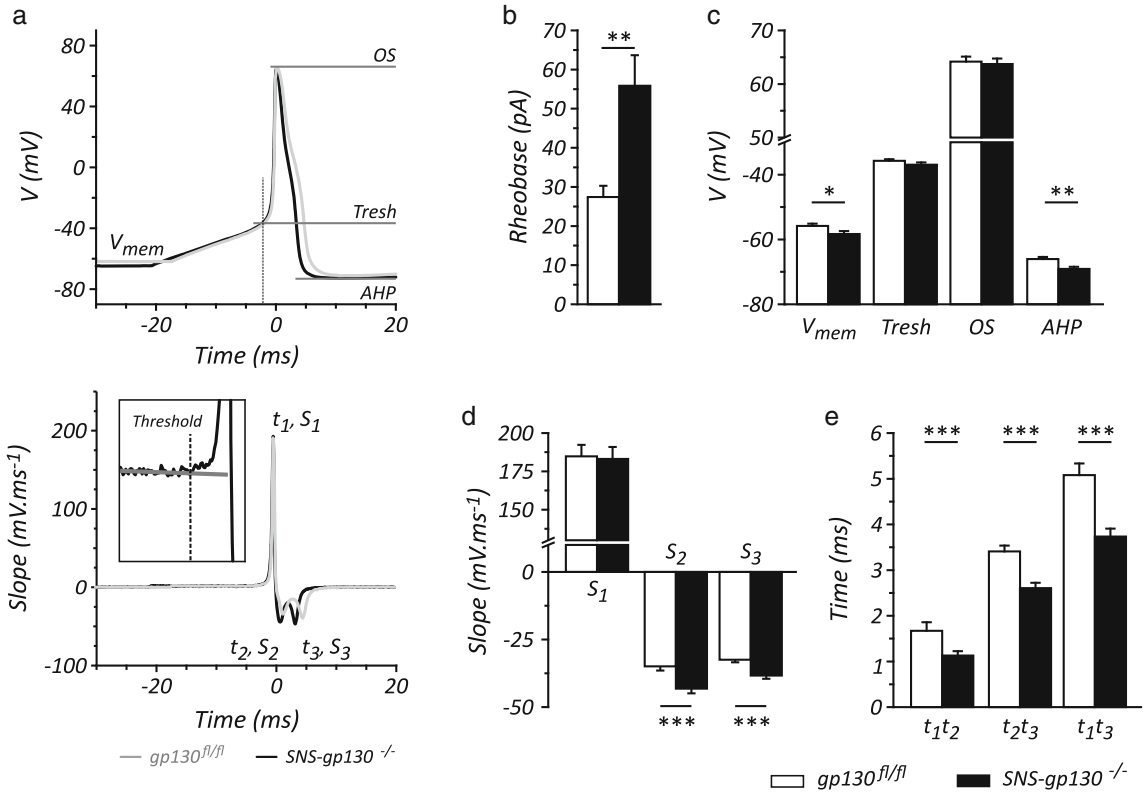

Fig. 1 Action potentials (APs) from SNS-$gp130^{-/-}$ DRGs show increased kinetics compared to $gp130^{fl/fl}$. **a** Typical AP recording from $gp130^{fl/fl}$ (*grey trace*) and SNS-$gp130^{-/-}$ (*black trace*) DRG neuron and its 1st derivative from which the parameters were extracted that are described in the "Materials and methods" section. **b** SNS-$gp130^{-/-}$ (*black bar*) requires a higher current injection to evoke an AP compared to $gp130^{fl/fl}$ DRG neurons (*white bar*, Mann–Whitney U test p=0.0012). **c** The membrane potential (V_{mem}) and afterhyperpolarization (*AHP*) of SNS-$gp130^{-/-}$ are significantly reduced (Student's t test, $^{*}p$=0.033 and Mann–Whitney U test, $^{**}p$=0.006, respectively), whereas the AP threshold (*Tresh*) and the overshoot (*OS*) are similar to $gp130^{fl/fl}$. **d** The depolarization speed (S_1) of APs are comparable in both SNS-$gp130^{-/-}$ and $gp130^{fl/fl}$, but both repolarization phases (S_2 and S_3) of SNS-$gp130^{-/-}$ are increased in speed (Mann–Whitney U test, $^{***}p$<0.001 for S_2 and Student's t test, $^{***}p$<0.001 for S_3). **e** The duration of the different phases of the AP in SNS-$gp130^{-/-}$ DRG neurons are all significantly reduced compared to $gp130^{fl/fl}$ neurons, resulting in a shorter AP width (t_1–t_3) in SNS-$gp130^{-/-}$ neurons (Mann–Whitney U test; $^{***}p$<0.001)

Table 2 Extracellular solutions used for general excitability and specific ionic conductance

	NaCl	NMDG	CsMeS	CsCl	KCl	TEACl	$CaCl_2$	$MgCl_2$	HEPES	Glucose
I_{all}	150	–	–	–	5	–	2	1	10	10
I_{Na^+}	90	–	50	–	–	10	2	1	10	10
I_{K^+}	–	145	–	–	5	–	2	1	10	10
$I_{Ca^{2+}}$	–	130	–	5	–	10	2	1	10	20

NMDG N-Methyl-D-glucamine, *CsMeS* cesium methanesulfonate, *TEACl* tetraethylammonium chloride

Concentrations are given in mM, pH of all external solutions were set to 7.3 with NaOH (*I*), CsOH (I_{Na}^+) or HCl (I_K^+ and I_{Ca}^{2+})

determined by a series of hyperpolarizing current injections from a holding current of 0 pA. The average resistance was calculated according to Ohm's law. From the AP evoked by injecting depolarizing current pulses, the resting membrane potential (V_{mem}), afterhyperpolarization (AHP), and overshoot (OS) of $gp130^{fl/fl}$ and SNS-$gp130^{-/-}$ DRG neurons were determined (Fig. 1a). The maximal speed of depolarization and repolarization, which could be discriminated into two different phases, was derived from the 1st derivative of the original AP. For determination of the AP threshold (Tresh), the time was determined where in the falling slope of the 1st derivative reversed into a rising slope (see Fig. 1a)

Voltage-gated sodium channels

Peak inward currents derived from voltage step protocol (from -80 to +80 mV for 50 ms), preceeded by a -120 mV hyperpolarizing pulse of 250 ms, were plotted against voltage and were fitted with a modified Boltzmann equation:

$$I_{Na} = I_{leak} + G(1/((1 + e((V\text{-}V_{act})/S))))(V\text{-}V_r)$$

where G is the conductance, I_{leak} is the leakage current at -80 mV, V_{act} is half maximal activation of the inward current, S the slope factor at V_{act}, and V_r is the reversal potential.

Voltage-gated calcium channels

Voltage-gated Ca^{2+} currents were evoked by 250 ms depolarizing pulses from -80 to +60 mV. Peak inward currents were determined as the maximal current within the first 50 ms. The measured currents were plotted against the stimulation voltage and fitted with a combined Boltzmann and Goldman–Hodgkin–Katz equation.

$$I_{Ca} = I_{leak} + G\left(\frac{1}{1 + \exp\left(-\frac{V\text{-}V_{act}}{S}\right)^2}\right)\left(\frac{1-\exp-\left(\frac{V\text{-}V_r}{25.5}\right)}{1-\exp-\left(\frac{V}{25.5}\right)}\right)$$

where in G is the conductance, I_{leak} is the leakage current at -80 mV, V_{act} is half maximal activation of the inward current, S the slope factor at V_{act}, and V_r is the reversal potential.

Voltage-gated potassium channels

Potassium currents were activated through 300 ms depolarizing pulses from -80 to +40 mV that were preceded by a hyperpolarizing pulse of -120 mV. Peak outward currents were determined as the maximal current within the first 50 ms, and the sustained current as average of last 25 ms. The resulting *IV* plots were fitted with a modified Boltzmann equation in which V_r was set to the Nernst equilibrium of K^+ (-86 mV)

$$I_K = I_{leak} + G\left(\frac{1}{1 + \exp\left(-\frac{V\text{-}V_{act}}{S}\right)}\right)(V\text{-}(V_r))$$

Activation of K^+ ionic currents at 0 mV were fitted with a single (4-AP sensitive currents) or double exponential (Ctrl and 4-AP resistant currents) function.

Single exponential:

$$I_K = A\exp\left(\frac{t}{t_1}\right) + I_{Kmax}$$

Double exponential:

$$I_\kappa = A\exp\left(\frac{t}{t_1}\right) + B\exp\left(\frac{t}{t_2}\right) + I_{Kmax}$$

where t_1 and t_2 are the time constants of activation, A and B are the respective current fraction (scaling parameters of the current amplitudes), and I_{Kmax} is the maximal K^+ current amplitude recorded at 0 mV.

qRT-Taqman PCR

For quantitative analysis of mRNA levels, total RNA was isolated from murine DRG cultures by using TRI Reagent (Sigma Aldrich) or peqGOLD TriFast (PeqLab) as previously published [5]. The quantity of RNA was analyzed using the Nanodrop 2000 (Thermo Scientific). Reverse transcription to cDNA was performed using 9 μl of total RNA and Mulv Reverse transcriptase (2.5 U/μl, Applied Biosystems) with Random Hexamer primers (10 ng/μl), RiboLock (2 U/μl), 1× Taq Buffer (Thermo Scientific), MgCl2 (5 mM), and dNTPs (1 mM, Fermentas) in a total volume of 20 μl per sample. cDNA samples were analyzed for expression of target genes by quantitative RT (qRT)-PCR using TaqMan 5′ nuclease assays (Applied Biosystems). Following assays were used: Mm01352363_m1 (succinate dehydrogenase subunit A, *Sdha*); Mm00434584_s1 (potassium voltage-gated channel, shaker-related subfamily, member 2, *Kcna2*); Mm01336166_m1 (potassium voltage-gated channel, shaker-related subfamily, member 4, *Kcna4*); Mm01302126_m1 (potassium voltage-gated channel, Shal-related subfamily, member 3, *Kcnd3*); and Mm01316769_m1 [potassium voltage-gated channel, subfamily H (Eag-related), member 1, *Kcnh1*]. Reactions were performed in a MicroAmp Fast Optical 96-well reaction plate (Applied Biosystems) using the 7500 Fast RT-PCR system (Applied Biosystems) for thermal cycling and real-time fluorescence measurements. The PCR cycle protocol consisted of 10 min at 95 °C, and 50 two-step cycles of 15 s each at 95 °C and of 1 min at 60°. Positive and negative controls (no-template controls for RT-PCR and TaqMan-qPCR) were included in the experiments. Each sample was run in triplicate for each TaqMan-qPCR. Threshold cycle (CT) values were recorded as a measure of initial template concentration. Relative fold changes in RNA levels were calculated by the ΔΔCT-method using SDHA as a reference standard. The range for the target was calculated by 2-ΔΔCT relative to $gp130^{fl/fl}$ samples as calibrator and data were normalized per experimental day.

Statistical analysis

Data are presented as mean ± SEM. For detailed statistical analysis the Sigmastat 3.0 (Aspire Software International) software package was used and Mann–Whitney *U* test or Student's *t* test were calculated. Differences were considered statistically significant at $p<0.05$.

Results

Decreased neuronal excitabilty of neurons from SNS-$gp130^{-/-}$ mice

Electrophysiological experiments were performed on primary sensory neurons 18 to 28 h after plating. Prior to each recording, the identity of the cells was confirmed by live-cell labeling with a gp130-specific antibody. In current clamp, the resting membrane potential of SNS-$gp130^{-/-}$ neurons was significantly lower than the resting membrane potential of $gp130^{fl/fl}$ neurons (SNS-$gp130^{-/-}$; -58.33±0.89 mV, n=62 vs. $gp130^{fl/fl}$; -55.84±0.73 mV, n=67; Mann–Whitney *U* test, p=0.0012), whereas the input resistance was unchanged ($gp130^{fl/fl}$; 1.15±0.08 GΩ, n=41 vs. SNS-$gp130^{-/-}$; 1.36±0.11 GΩ, n=44, respectively). APs were evoked in $gp130^{fl/fl}$ and SNS-$gp130^{-/-}$ DRG neurons by stepwise increasing current injections. The SNS-$gp130^{-/-}$ neurons had a markedly increased rheobase (the minimal amount of current input to evoke a single AP) of 55.85±7.79 pA (n=47) compared to control $gp130^{fl/fl}$ with 27.41±2.78 pA (n=47). The OS of the evoked APs and the upstroke velocity (S_1) of SNS-$gp130^{-/-}$ were similar to $gp130^{fl/fl}$ (Table 3). The threshold of the AP evoked by current injection was derived from the 1st derivative of the voltage recording. The time point where the slight declining phase converted into an 'irreversible' increasing phase (see inset) was determined and the corresponding voltage was deducted from the original voltage recording. We did not observe a difference in the AP thresholds of both $gp130^{fl/fl}$ and SNS-$gp130^{-/-}$ DRG neurons (Table 3). The repolarization phase of the AP in DRG neurons consisted of two distinct phases, exhibiting a "hump" in the falling phase of AP, typical for small nociceptors [39, 44]. These two phases were represented by two distinct peaks in the differentiated voltage recording (Fig. 1; S_2 and S_3, Table 3). In nociceptors lacking gp130, the first phase of repolarization was significantly faster compared to gp130 expressing $gp130^{fl/fl}$ nociceptors (-43.19±1.73 mV ms^{-1}, n=62 vs. -34.92±1.58 mV ms^{-1}, n=67, respectively). In addition, the 2nd phase of repolarization occurred also with greater speed in SNS-$gp130^{-/-}$ neurons than in $gp130^{fl/fl}$ neurons (-38.31±1.23 mV ms^{-1}, n=62 vs. -32.49±0.93 mV ms^{-1}, n=67). Finally, the AHP amplitude of $gp130^{fl/fl}$ neurons was significantly higher than the AHP of SNS-$gp130^{-/-}$ neurons ($gp130^{fl/fl}$ -66.06±0.66 mV, n=67 and SNS-$gp130^{-/-}$ -69.07±0.66 mV, n=62).

As the depolarization and repolarization speed of the AP set the width of the AP, we determined the time intervals between the three "peaks" from the derivative of the AP. In accordance to the increased repolarization speed of APs of SNS-$gp130^{-/-}$ nociceptors, all time intervals were significantly reduced in SNS-$gp130^{-/-}$ compared to control neurons (see Table 4 and Fig. 1a).

Voltage-gated sodium and calcium currents are unaltered in SNS-$gp130^{-/-}$ neurons

An altered resting membrane potential, rheobase, and repolarization should be reflected in an altered activity of ion channels. Therefore, the different currents involved in the AP were analyzed. In nociceptors, both TTX-sensitive and TTX-

Table 3 Action potential characteristics of gp130$^{fl/fl}$ and SNS-gp130$^{-/-}$ nociceptive neurons

	RMP (mV)	IR (GΩ)	Rheobase (pA)	OS (mV)	Threshold (mV)	AHP (mV)
gp130$^{fl/fl}$	-55.84±0.73*	1.15±0.08	27.41±2.78**	64.19±0.93	-35.73±0.52	-66.06±0.66**
SNS-gp130$^{-/-}$	-58.33±0.89	1.36±0.11	55.85±7.79	63.73±1.03	-36.95±0.71	-69.07±0.66

RMP resting membrane potential, *IR* input resistance, *OS* overshoot, *AHP* afterhyperpolarization

* $p<0.05$ and ** $p<0.01$; for details, see Fig. 1

resistant sodium channels are expressed [1, 2, 42, 49]. The DRG neurons were kept at a holding potential of -80 mV, and sodium currents were evoked by stepwise depolarizations between -80 and +80 mV, preceeded by a 250 ms hyperpolarizing pulse of -120 mV. The total peak current amplitudes were plotted in an *IV* curve and fitted with a modified Boltzmann equation (see "Materials and methods" section). A typical recording of sodium currents (Fig. 2a, upper panel) and the average *IV* plot of a gp130$^{fl/fl}$ neuron is depicted in Fig. 2b. The neurons derived from gp130$^{fl/fl}$ mice had an average sodium conductance of 4.84±0.26 nS/pF (n=36). The sodium currents activated half maximally at -37.26± 0.99 (n=36) with a steep slope in the *IV* relationship (slope factor; 1.77±0.16, n=36). Voltage-gated sodium currents from SNS-gp130$^{-/-}$ neurons were indistinguishable from those of gp130$^{fl/fl}$ neurons. The inward Na^+ currents in both types of neurons was maximal at -35 mV (gp130$^{fl/fl}$; -358.75±25.72 pA pF^{-1}, n=36, SNS-gp130$^{-/-}$; -399.36±32.45 pA pF^{-1}, n=32) and reversed around +50 mV (gp130$^{fl/fl}$; 53.67±0.63 mV, n= 36, SNS-gp130$^{-/-}$; 51.85±0.92 mV, n=32). The size-corrected Na^+ conductance of SNS-gp130$^{-/-}$ nociceptors amounted to 5.38±0.29 nS/pF (n=32). Furthermore, SNS-gp130$^{-/-}$ neurons had a similar V_{act} and were equally fast in activation (V_{act}; -40.00±1.35 mV and slope factor; 1.82±0.26, n=32; Fig. 2c).

To discriminate between the different types of sodium currents, TTX-sensitive channels were blocked by 250 nm TTX. The TTX-resistant sodium currents were analyzed as described above. The conductance of TTX-resistant voltage-gated sodium currents was comparable between gp130$^{fl/fl}$ and SNS-gp130$^{-/-}$neurons (gp130$^{fl/fl}$; 3.59±0.30 mV, n=29 vs. SNS-gp130$^{-/-}$; 3.81±0.30 mV, n=30). Furthermore, the half maximal activation derived from the *IV* plot was indistinguishable between both types of DRG neurons (gp130$^{fl/fl}$; -23.78±1.31 mV, n=29 vs. SNS-gp130$^{-/-}$ V_{act}; -26.00±0.32 mV, n=30). These results suggest that difference in excitabilty is unlikely due to different kinetics of voltage-gated sodium currents in gp130$^{fl/fl}$- and SNS-gp130$^{-/-}$-derived neurons.

In small-sized sensory neurons, voltage-gated Ca^{2+} currents shape the AP. Therefore, voltage-dependent calcium channels were assessed and the inward peak currents analyzed. In both genotypes, the high voltage-activated Ca^{2+} currents had an equal activation voltage (V_{act}, Table 5) and slope factor (S, Table 5). Furthermore, the peak inward calcium conductance of SNS-gp130$^{-/-}$ nociceptors was equal to gp130$^{fl/fl}$ neurons (G, Table 5). In 4 out of 19 SNS-gp130$^{-/-}$ nociceptors, we observed the presence a low voltage-activated Ca^{2+} current, comparable to the 5/22 of gp130$^{fl/fl}$ neurons. Despite the small numbers of nociceptors displaying T-type Ca^{2+} currents, there were no obvious differences observed in the biophysical properties of the *IV* plots of both genotypes (data not shown).

Augmentation of voltage-gated potassium currents in gp130$^{-/-}$ neurons

Potassium channels are crucial for the repolarization of the AP. Since the speed of repolarization was significantly increased in SNS-gp130$^{-/-}$ neurons, we suspected that altered potassium currents could be the reason. It is generally accepted that the repolarization phase of APs of nociceptors has two separate phases, which are due to activation of different subfamilies of potassium channels. The fast repolarization is predominantly carried by A-type voltage-gated potassium

Table 4 Upstroke and repolarization velocities, and time constants of 1st derivation of action potentials recorded from gp130 expressing and gp130-deficient nociceptors (explanation in the text)

	S_1 (mV ms^{-1})	S_2 (mV ms^{-1})	S_3 (mV ms^{-1})	t_1–t_2 (ms)	t_2–t_3 (ms)	t_1–t_3 (ms)
gp130$^{fl/fl}$ n=67	184.81±7.49	-34.92±1.58 ***	-32.49±0.93 ***	1.67±0.19 ***	3.41±0.13 ***	5.08±0.26 ***
SNS-gp130$^{-/-}$ n=62	183.10±7.84	-43.19±1.73	-38.31±1.23	1.13±0.10	2.61±0.12	3.73±.018

S_1 Upstroke velocity, S_2 1st repolarization velocity, S_3 2nd repolarization velocity, t_1–t_2 time interval between S_1 and S_2, t_2–t_3 time interval between S_2 and S_3, t_1–t_3 time interval between S_1 and S_3

*** $p<0.001$, for details, see Fig. 1

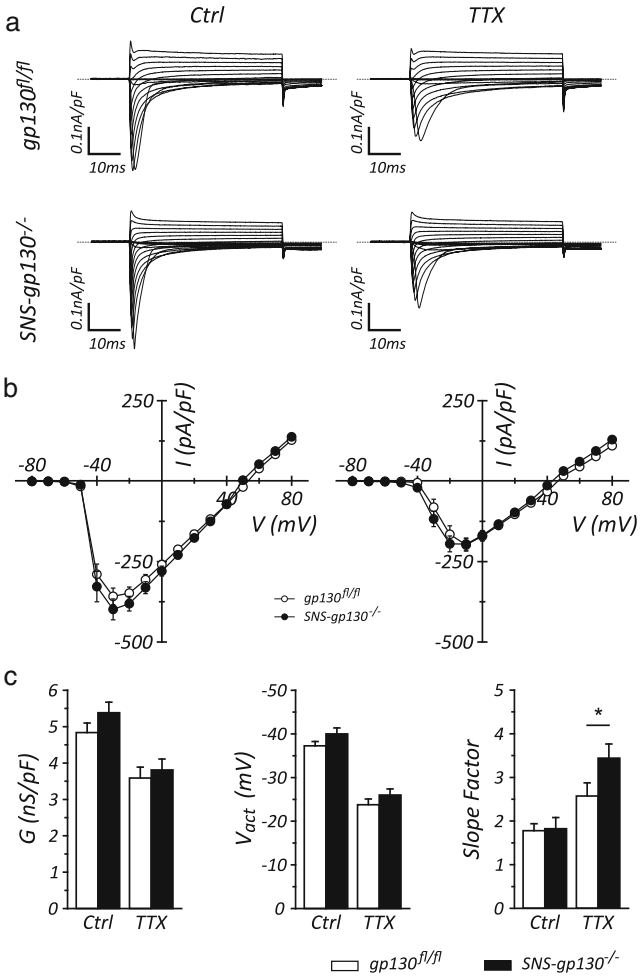

Fig. 2 Voltage-gated sodium currents in gp130$^{fl/fl}$ and SNS-gp130$^{-/-}$ DRG neurons are indistinguishable. **a** Typical recordings of voltage-gated sodium currents in gp130$^{fl/fl}$ (*upper traces*) and SNS-gp130$^{-/-}$ (*lower traces*) under control (*left traces*) and TTX (*right traces*) conditions. **b** The Na^+-*IV* plots derived from Na^+ current recordings of gp130$^{fl/fl}$ (*white circles*) and SNS-gp130$^{-/-}$ DRG neurons (*black circles*) are similar in both control condition (left *IV* plot) and after application of TTX (right *IV* plot). No differences in the current density is observed between the two DRG neuron populations. **c** The conductance (*G*) and the half-maximal activation voltage (V_{act}) obtained after fitting of the individual *IV* plots do not show a difference between gp130$^{fl/fl}$ (*white bars*) and SNS-gp130$^{-/-}$ neurons (*black bars*). The obtained slope factor in SNS-gp130$^{-/-}$ is slightly increased in the TTX-resistant Na^+ *IV* plot (Student's *t* test, $^*p=0.022$), and the slope factor of the *IV* plot of TTX-sensitive and TTX-resistant Na^+ currents are comparable

channels. These channels exhibit fast activation and inactivation properties and can be blocked by 4-AP [53, 59]. The slow repolarization is mainly due to the activity of different types of delayed rectifier potassium channels. Therefore, peak and sustained potassium currents were analyzed. Both peak and sustained potassium *IV* plots were fitted with a Boltzmann-like equation (see "Materials and methods" section). It could be shown that both voltage-dependent peak and sustained potassium currents of SNS-gp130$^{-/-}$ neurons were significantly greater at higher voltages compared to the respective currents in gp130$^{fl/fl}$ control (I_{peak}: 0.55±0.03 nA pF^{-1}, n=18 vs. 0.45±0.03 nA pF^{-1} at 40 mV, n=17; and I_{sus}: 0.48±0.03 nA pF^{-1}, n=18 and 0.39±0.03 nA pF^{-1} at 40 mV, n=17; Student's *t* test, $^*p<0.05$). In accordance with these results, the size-corrected peak potassium conductance of SNS-gp130$^{-/-}$ is significantly greater than of gp130$^{fl/fl}$ (Fig. 3a, 3.96±0.29 nS pF^{-1}, n=17 and 4.98±0.29 nS pF^{-1}, n=18, respectively; Student's *t* test, $^*p<0.05$). However, the conductance of the sustained potassium currents was not different to the gp130$^{fl/fl}$ (3.54±0.28 nS pF^{-1}) and SNS-gp130$^{-/-}$ (4.29±0.310 nS pF^{-1}). The voltage of half maximal activation derived from the curve fitting were also comparable between both types of neurons (Table 6).

To investigate the 4-AP-insensitive K^+ current, 4-AP (5 mM) was used to isolate the delayed rectifier K^+ channels. SNS-gp130$^{-/-}$ nociceptors still displayed a significant larger current at positive voltages (Fig. 4). Accordingly, SNS-gp130$^{-/-}$ DRG neurons had larger size-corrected peak and sustained conductances than gp130$^{fl/fl}$ DRG neurons (SNS-gp130$^{-/-}$ vs. gp130$^{fl/fl}$; G_{peak} 3.69±0.28 nA pF^{-1}, n=10 vs. 2.75±0.23 nA pF^{-1}, n=12; and G_{sus} 3.46±0.30 nS pF^{-1}, n=10 vs. 2.68±0.22 nS pF^{-1}, n=12) as derived from curve fitting. Despite the difference in conductance, no difference in activation voltage and slope of activation of the 4-AP-resistant K^+–*IV* curves was observed between gp130$^{fl/fl}$ and SNS-gp130$^{-/-}$ nociceptors.

The 4-AP-sensitive current was derived by subtraction of the 4-AP-insensitive K^+ currents from control K^+ currents. In gp130-deficient nociceptors, the 4-AP-sensitive K^+ peak current was significantly larger compared to the peak outward K^+ current measured in gp130$^{fl/fl}$ neurons at +40 mV (0.29±0.03 nA pF^{-1}, n=11 and 0.18±0.02 nA pF^{-1}, n=12, respectively, Student's *t* test, ** $p<0.01$). Hence, the outward peak conductance of the 4-AP recorded current was significantly larger (2.69±0.45 nS pF^{-1}, n=11 and 1.51±0.18, n=12 respectively, Student's *t* test, *$p<0.05$) in SNS-gp130$^{-/-}$ nociceptors. The activation kinetics as derived from *IV* fitting did not yield a difference between both gp130$^{fl/fl}$ and SNS-gp130$^{-/-}$ nociceptors (Table 6).

Table 5 Biophysical properties of voltage-gated Ca^{2+} currents in gp130$^{fl/fl}$ and SNS-gp130$^{-/-}$ DRG neurons

Genotype	*N*	*G* (nS/pF)	V_{act} (mV)	*S*	V_r (mV)
gp130$^{fl/fl}$	24	0.53±0.05	-15.03±0.55	4.78±0.31	50.11±1.27
SNS-gp130$^{-/-}$	19	0.61±0.0.04	-17.10±0.76	4.98±0.33	49.16±0.96

G Cellular Ca^{2+} conductance, V_{act} activation voltage, *S* slope factor at V_{act}, V_r reversal potential

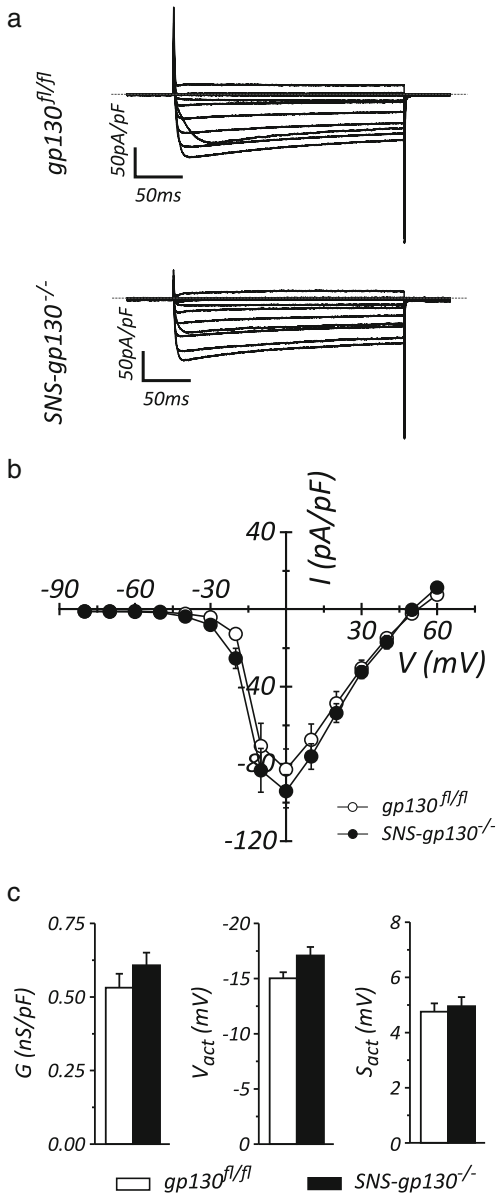

Fig. 3 In gp130$^{fl/fl}$ and SNS-gp130$^{-/-}$ DRG neurons, voltage-gated calcium currents are comparable. **a** Typical recordings of voltage-gated calcium currents in gp130$^{fl/fl}$ (*upper traces*) and SNS-gp130$^{-/-}$ (*lower traces*). **b** The Ca^{2+}-*IV* plots derived of the peak Ca^{2+} current obtained from gp130$^{fl/fl}$ (*white circles*) and SNS-gp130$^{-/-}$ DRG neurons (*black circles*) are similar. In the Ca^{2+} current density, no obvious differences are observed between gp130$^{fl/fl}$ and SNS-gp130$^{-/-}$ DRG neuron populations. **c** Parameters derived from *IV* fitting of peak inward Ca^{2+} currents from both gp130-expressing (*white bars*) and gp130-deficient nociceptors (*black bars*) did not reveal significant alterations in activation kinetics

In addition to the K+*IV* analysis, the activation kinetics of 4-AP-resistant (4-AP Res) and 4-AP-sensitive (4-AP Sens) currents were calculated for depolarizations evoked at 0 mV. The 4-AP Res currents were fitted with a double exponential to determine the time constants of activation of K^+ currents. Both activation time constants t_1 and t_2 of K^+ currents were smaller in SNS-gp130$^{-/-}$ neurons than in gp130$^{fl/fl}$ neurons (Table 7). The deduced 4-AP Sens currents could be fitted with a single exponential equation. Similar to the 4-AP Res currents, the 4-AP-sensitive K^+ current of SNS-gp130$^{-/-}$ nociceptors evoked at 0 mV activated faster than in gp130$^{fl/fl}$, depicted by a smaller t_1 (Table 7).

Neurons from SNS-gp130$^{-/-}$mice expressing significantly higher levels of Kcna4

On the basis of the electrophysiological results, an increased expression of voltage-gated K^+ channels was to be anticipated. Therefore, gene expression levels of possible candidates were assessed using quantitative Taqman RT-PCR. In neuropathic pain states, the expression of Kv1.2 (*Kcna2*), Kv1.4 (*Kcna4*), and Kv4.3 (*Kcnd3*) giving rise to K^+ currents was reduced, and this is generally associated with nociceptor hyperexcitability [64, 66, 67]. Recently, our experiments indicated that Kv10.1 (*Kcnh1*) expression in SNS-gp130$^{-/-}$ is differentially expressed in DRG explants (data not shown). Therefore, the mRNAs of *Kcna2*, *Kcna4*, *Kcnd3*, and *Kcnh1* were analyzed in cultures of gp130$^{fl/fl}$ and SNS-gp130$^{-/-}$ nociceptors. The mRNA of all four K^+ channels were detectable in gp130$^{fl/fl}$ and SNS-gp130$^{-/-}$ nociceptors. Strikingly, only the expression of *Kcna4* was significantly higher in SNS-gp130$^{-/-}$ DRG neurons (1.34±0.10, n=7, Mann–Whitney U test, $p<0.05$), whereas the *Kcna2*, *Kcnd3* showed a nonsignificant increase in expression, and *Kcnh1* mRNA expression levels were similar in both genotypes (Fig. 5b). These data suggest that expression of A-type *Kcna4* channels may be regulated by gp130 which seemingly acts as a break for the expression of *Kcna4* to increase noceptor excitability in pain states associated with local or general inflammation.

Discussion

Our results point out to a deficit in excitability of small-sized nociceptive neurons in acute primary cultures obtained from mice with a conditional null mutation of the cytokine signal transducer gp130 in nociceptive neurons. The hyperpolarized resting potential and alterations in kinetics within specific subsets of voltage-gated ionic currents obtained from gp130-deficient neurons are in line with an increased expression of *Kcna4* channels, but little or no alteration of Na^+ and Ca^{2+} channels.

In general, neurons require voltage-gated ion channels for AP generation and propagation, and they regulate conductances of Na^+, Ca^{2+}, and K^+ ions. In particular, sodium and calcium channels have been intensely studied and are generally accepted to contribute to changes in the pain pathway that are associated with increased pain sensitivity [17, 19, 24, 42]. The TTX-sensitive NaV1.7 is a major candidate to amplify submaximal depolarizations due to its slow inactivation and

Table 6 Biophysical properties of voltage-gated K^+ currents derived from the *IV* plot in cultivated nociceptors derived fom gp130$^{fl/fl}$ and SNS-gp130$^{-/-}$ DRGs

		gp130$^{fl/fl}$ (n=17)		SNS-gp130$^{-/-}$ (n=17)	
		I_{peak}	I_{sus}	I_{peak}	I_{sus}
V_{act} (mV)	Control	-2.10±2.08	-2.64±1.96	-4.91±1.47	-5.21±1.36
	4-AP Res	1.69±3.76	-3.93±3.36	-5.33±2.06	-8.43±1.63
	4-AP Sens	-7.88±3.62	–	-7.53±4.48	–
Slope factor	Control	19.36±0.77	20.20±0.87	21.98±1.11	21.13±0.58
	4-AP Res	19.91±0.77	19.85±0.97	20.53±0.74	21.31±0.76
	4-AP Sens	14.92±1.09	–	16.81±1.86	–

I_{peak} K^+ peak outward current, I_{sus} K^+ sustained outward current, V_{act} activation voltage, *4-AP Res* K^+ currents insensitive to 4-AP, *4-AP Sens* K^+ currents sensitive to 4-AP inhibition

thereby brings the neuron closer to its AP threshold [18]. Mutations within the *Scn9a* gene encoding NaV1.7 change pain perception [21, 42, 45]. The TTX-sensitive NaV1.3 sodium channel is solely expressed during embryonic stages. However, neuropathic pain or peripheral nerve injury can cause re-expression of NaV1.3 channels in DRG neurons [9]. Similar to NaV1.7, NaV1.3 channels can be involved in high frequency AP generation or in amplification of

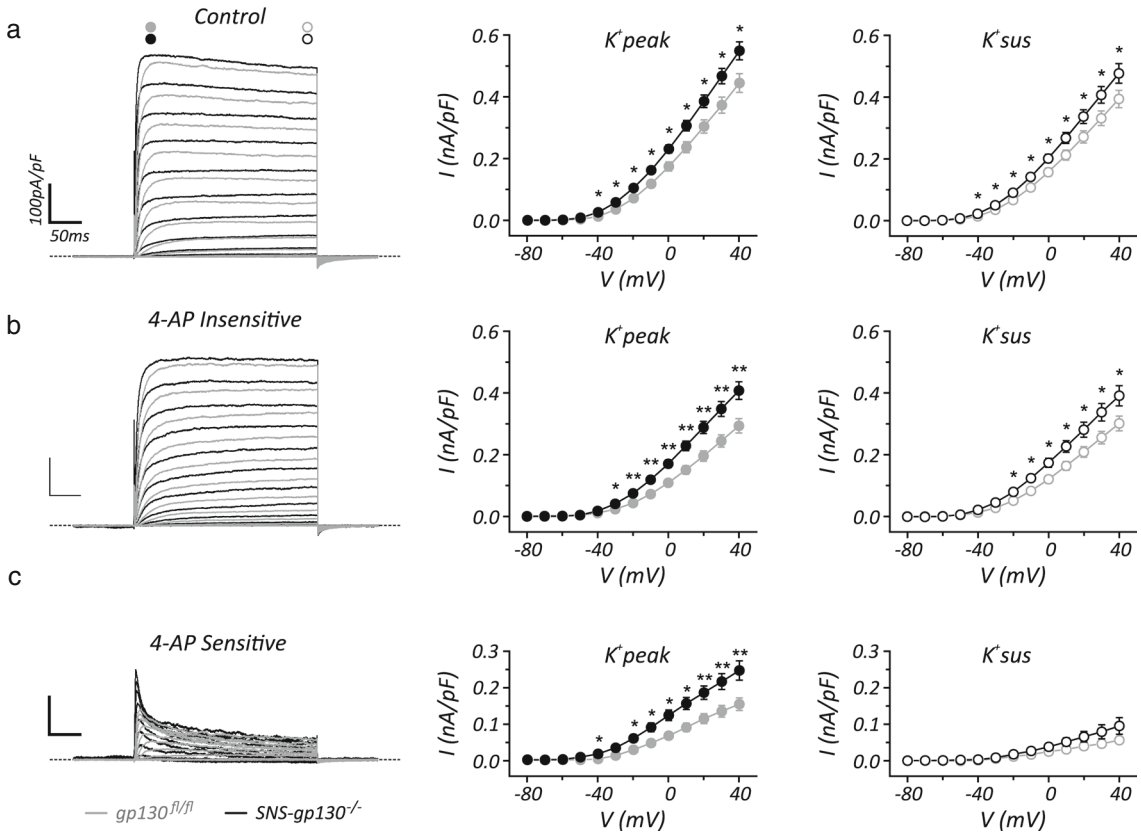

Fig. 4 Voltage-gated potassium currents are increased in gp130-deficient nociceptors. **a** Recordings of voltage-gated K^+ current in gp130$^{fl/fl}$ (*grey traces*) and in SNS-gp130$^{-/-}$ (*black traces*) DRG neurons. Both K_{peak} (*filled black circles*) and K_{sus} (*open black circles*) current densities are significantly increased in the gp130-deficient nociceptors compared to the current denisties recorded in gp130$^{fl/fl}$ (K_{peak} *filled grey circles*, K_{sus} *open grey circles*) neurons, Student's *t* test, $^*p<0.05$. **b** and **c** Both K^+ peak current densities of 4-AP-insenstive (**b**) and 4-AP-sensitive K^+ currents (**c**) are increased in SNS-gp130$^{-/-}$ neurons as evident from the *IV* plots (*middle panel*, Student's *t* test, $^*p<0.05$, $^{**}p<0.01$). However, only the sustained K^+ current density is only increased in 4-AP-insentive K^+ current in SNS-gp130$^{-/-}$ neurons (**b** *right panel*, *black open circles*, $^*p<0.05$) at high positive voltages. No differences are observed in the sustained K^+ current of 4-AP-sensitive current (**c** *right panel*)

Table 7 Activation time constants of voltage-gated K^+ currents evoked at 0 mV in cultivated nociceptors derived fom $gp130^{fl/fl}$ and SNS-$gp130^{-/-}$ DRGs

	$gp130^{fl/fl}$			SNS-$gp130^{-/-}$		
	N	t_1 (ms)	t_2 (ms)	*N*	t_1 (ms)	t_2 (ms)
Control	18	6.16±0.79***	29.93±8.48*	17	2.80±0.36	12.03±2.86
4-AP Res	12	29.63±9.33**	150.85±28.78**	10	6.53±0.90	33.13±7.51
4-AP Sens	12	4.48±0.66***	–	10	1.67±0.22	–

4-AP Res K^+ currents insensitive to 4-AP

4-AP Sens K^+ currents sensitive to 4-AP inhibition

*$p<0.05$, **$p<0.01$, and ***$p<0.001$, Mann–Whitney *U* test, all compared to the according SNS-$gp130^{-/-}$ parameter

subthreshold depolarizations [41]. Besides the TTX-sensitive Na^+ channels, the TTX-resistant NaV1.8 channel is of importance in repetitive firing at prolonged depolarizations. Furthermore, in DRG neurons, they are the main contributors to the Na^+ influx in the upstroke of the AP [56]. In the current study, we did not observe any difference of threshold of the AP, OS, and speed of depolarization which could be correlated with voltage-gated sodium channel expression and function.

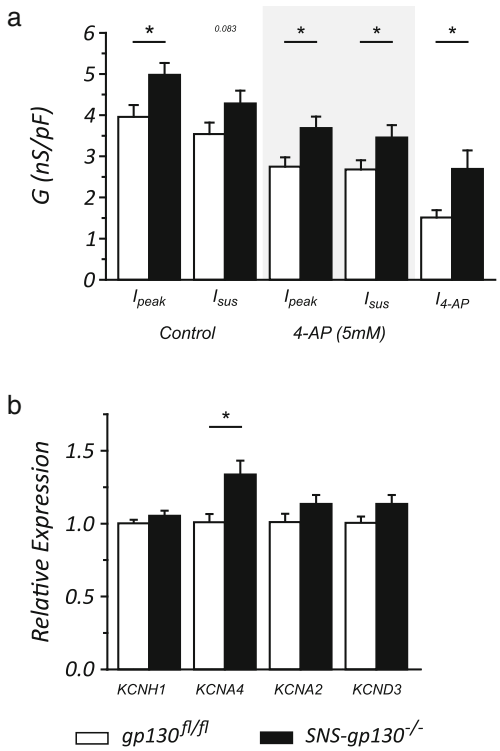

Fig. 5 SNS-$gp130^{-/-}$ DRG neurons have increased K^+ conductances that coincides with increased expression of voltage-gated K^+ channels. **a** All K^+ conductances (*G*) derived from *IV* fitting fo the peak K^+ currents (I_{peak}) are augmented in SNS-$gp130^{-/-}$ DRG neurons (*black bars*) compared to $gp130^{fl/fl}$ neurons (*white bars*). Futhermore, the 4-AP sustained K^+ conductance (I_{sus}) is only elevated in the 4-AP-insensitive fraction (Student's *t* test, *$p<0.05$). **b** SNS-$gp130^{-/-}$ nociceptors (*black bars*) exhibit higher expression of Kv1.4 (KCNA4) than $gp130^{fl/fl}$ DRG neurons (*white bars*). Expression of Kv1.2 (KCNA2), Kv4.3 (KCND3), and Kv10.1 (KCNH1) mRNA was similar between both genotypes (Mann–Whitney *U* test, *< 0.05)

Furthermore, in-depth recordings in $gp130^{fl/fl}$ and SNS-$gp130^{-/-}$ DRG neurons using ion replacement to isolate voltage-gated sodium channels did not show any differences in conductance or activation kinetics. We did not find any effects of SNS-Cre expression on the shape of the AP nor in biophysical properties of the TTX-resistant sodium channels, in line with recent findings that the AP properties of SNS-Cre mice do not differ from their wildtype littermates [62]. Therefore, we conclude that the reduced excitability of neurons obtained from SNS-$gp130^{-/-}$ mice is likely due to changes in voltage-gated ion channels other than the NaV family of Na^+ channels.

Besides voltage-gated sodium channels, several types of Ca^{2+} channels are expressed in small- and medium-sized DRG neurons and sensory primary afferents [4, 63]. T-type calcium channels are already activated at voltages close to the resting membrane potential or by small membrane depolarization and thereby can regulate AP shape and discharge patterns [33]. T-type calcium currents are increased after nerve lesion in small DRG neurons [35], and inhibition of the T-type calcium channels results in reduction of thermal hypersensitivity and reduced pain responses in the formalin test [15, 51]. The N-type Ca^{2+} channels control synaptic transmission of C and Aδ fibers in pain processing. However, after nerve lesion, alternative splicing of N-type Ca^{2+} channels may alter their function. Moreover, the splice variant exon37a has attracted special interest because it is exclusively expressed in capsaicin-sensitive DRG neurons [8] and is selectively involved in mechanical and thermal hypersensitivity in inflammatory and neuropathic pain [3]. Nevertheless, our data shows that calcium current properties were very similar in $gp130^{fl/fl}$ and SNS-$gp130^{-/-}$ nociceptors. We therefore reason that it is unlikely that calcium currents are causally involved in the reduced excitability of neurons lacking gp130.

The most striking differences between genotypes were observed in voltage-gated potassium currents. Potassium channels in DRG neurons are important not only for AP repolarization but also for setting resting membrane potential and firing frequency upon excitation [29, 36, 37, 40]. Both AP repolarization and resting membrane potential were significantly altered in SNS-$gp130^{-/-}$ mice and could potentially account for the reduced DRG neuron excitability of these mice.

Adult DRG neurons express several delayed rectifier K^+ channels such as Kv1.2 and Kv10.1 [10, 55, 68]. The density of delayed rectifier K^+ currents is decreased in the chronic DRG compression model or after exposure to proalgesic endothelin-1, and therefore, they have been associated with the hyperexcitability of neurons [25, 26]. More recently, they have gained some interest as potential novel targets for pain treatment [22, 52, 61]. Surprisingly, our electrophysiological data point out to increased expression of delayed rectifier channels, however, regarding our two candidates; *Kcna2* (Kv1.2) expression was increased nonsignificantly in SNS-gp130$^{-/-}$ nociceptors, and *Kcnh1* (Kv10.1) was found undifferentially expressed in the current study.

A-type K^+ currents and the corresponding K^+ channels, e.g., Kv1.4 and Kv4.3, are regularly expressed in DRG neurons, where, e.g., Kv4.3 is predominantly expressed in small-sized C-fiber neurons [47, 53]. A-type K^+ currents contribute to normal mechanosensation, and reduced expression in nociceptors induces mechanical hypersensitivity [14, 66]. A-type K^+ channels set nociceptor sensitivity, and more specifically, cooling causes inhibition of A-type current in DRG neurons [58]. In addition, the A-type potassium channels are targeted by analgesic drugs like butamben or diclofenac [22, 65]. In the current study, we discovered a significant upregulation of *Kcna4* (Kv1.4) in gp130-deficient nociceptors, which was associated with augmented hyperpolarising K^+ currents and shortening of AP width. Since Kv1.4 gives rise to an A-type K^+ current and A-type currents are generally accepted to modify APs, we conclude that Kv1.4 is critically involved in the reduced excitability of gp130-deficient neurons.

The current data suggest that the presence of gp130 activates a break for the expression of the A-type K^+ channel gene *Kcna4*. The inhibition of Kcna4 by gp130 prevents the nociceptors to enter into a hypoexcitable state, in which nociceptors are less likely to generate APs. This suggests that gp130 is required to initiate neuron hypersensitivity. This, together with recent literature on potassium channels, sheds novel light on how the mechanism gp130 can induce and maintain pathological pain states [5, 11, 54, 57].

Acknowledgements The author would like to thank Kathrin Braun for preparing all the primary sensory neuron cultures. Furthermore, they would like to acknowledge Markus Doblander for assisting in breeding and genotyping of the mice. This project was supported by a grant from Fonds zur Förderung der wissenschaftlichen Forschung, Austria (FWF P18444) and the graduate program Signal Processing Neurons (SPIN W1206-B18).

References

1. Agarwal N, Offermanns S, Kuner R (2004) Conditional gene deletion in primary nociceptive neurons of trigeminal ganglia and dorsal root ganglia. Genesis 38:122–129. doi:10.1002/gene.20010, PMID: 15048809
2. Akopian AN, Sivilotti L, Wood JN (1996) A tetrodotoxin-resistant voltage-gated sodium channel expressed by sensory neurons. Nature 379:257–262. doi:10.1038/379257a0, PMID: 8538791
3. Altier C, Dale CS, Kisilevsky AE et al (2007) Differential role of N-type calcium channel splice isoforms in pain. J Neurosci 27:6363–6373. doi:10.1523/JNEUROSCI.0307-07.2007, PMID: 17567797
4. Altier C, Zamponi GW (2004) Targeting Ca^{2+} channels to treat pain: T-type versus N-type. Trends Pharmacol Sci 25:465–470. doi:10.1016/j.tips.2004.07.004, PMID: 15559248
5. Andratsch M, Mair N, Constantin CE et al (2009) A key role for gp130 expressed on peripheral sensory nerves in pathological pain. J Neurosci 29:13473–13483. doi:10.1523/JNEUROSCI.1822-09.2009, PMID: 19864560
6. Arvidson NG, Gudbjörnsson B, Elfman L et al (1994) Circadian rhythm of serum interleukin-6 in rheumatoid arthritis. Ann Rheum Dis 53:521–524, PMID: 7944637
7. Banner LR, Patterson PH (1994) Major changes in the expression of the mRNAs for cholinergic differentiation factor/leukemia inhibitory factor and its receptor after injury to adult peripheral nerves and ganglia. Proc Natl Acad Sci U S A 91:7109–7113, PMID: 8041754
8. Bell TJ, Thaler C, Castiglioni AJ et al (2004) Cell-specific alternative splicing increases calcium channel current density in the pain pathway. Neuron 41:127–138, PMID: 14715140
9. Black JA, Liu S, Tanaka M et al (2004) Changes in the expression of tetrodotoxin-sensitive sodium channels within dorsal root ganglia neurons in inflammatory pain. Pain 108:237–247. doi:10.1016/j.pain.2003.12.035, PMID: 15030943
10. Bocksteins E, Raes AL, Van de Vijver G et al (2009) Kv2.1 and silent Kv subunits underlie the delayed rectifier K^+ current in cultured small mouse DRG neurons. Am J Physiol Cell Physiol 296:C1271–C1278. doi:10.1152/ajpcell.00088.2009, PMID: 19357235
11. Boettger MK, Leuchtweis J, Kümmel D et al (2010) Differential effects of locally and systemically administered soluble glycoprotein 130 on pain and inflammation in experimental arthritis. Arthritis Res Ther 12:R140. doi:10.1186/ar3079, PMID: 20626857
12. Caterina MJ, Schumacher M a, Tominaga M et al (1997) The capsaicin receptor: a heat-activated ion channel in the pain pathway. Nature 389:816–824. doi:10.1038/39807, PMID: 9349813
13. Catterall W (2010) Ion channel voltage sensors: structure, function, and pathophysiology. Neuron 67:915–928. doi:10.1016/j.neuron.2010.08.021, PMID: 20869590
14. Chien L, Cheng J-K, Chu D et al (2007) Reduced expression of A-type potassium channels in primary sensory neurons induces mechanical hypersensitivity. J Neurosci 27:9855–9865. doi:10.1523/JNEUROSCI.0604-07.2007, PMID: 17855600
15. Choe W, Messinger RB, Leach E et al (2011) TTA-P2 is a potent and selective blocker of T-type calcium channels in rat sensory neurons and a novel antinociceptive agent. Mol Pharmacol 80:900–910. doi:10.1124/mol.111.073205, PMID: 21821734
16. Constantin CE, Mair N, Sailer CA et al (2008) Endogenous tumor necrosis factor alpha (TNFalpha) requires TNF receptor type 2 to generate heat hyperalgesia in a mouse cancer model. J Neurosci 28:5072–5081. doi:10.1523/JNEUROSCI.4476-07.2008, PMID: 18463260
17. Cregg R, Momin A, Rugiero F et al (2010) Pain channelopathies. J Physiol 588:1897–1904. doi:10.1113/jphysiol.2010.187807, PMID: 20142270
18. Cummins TR, Howe JR, Waxman SG (1998) Slow closed-state inactivation: a novel mechanism underlying ramp currents in cells expressing the hNE/PN1 sodium channel. J Neurosci 18:9607–9619, PMID: 9822722
19. Czeschik JC, Hagenacker T, Schäfers M, Büsselberg D (2008) TNF-alpha differentially modulates ion channels of nociceptive neurons. Neurosci Lett 434:293–298. doi:10.1016/j.neulet.2008.01.070, PMID: 18314270

20. DeLeo JA, Colburn RW, Nichols M, Malhotra A (1996) Interleukin-6-mediated hyperalgesia/allodynia and increased spinal IL-6 expression in a rat mononeuropathy model. J Interferon Cytokine Res 16: 695–700, PMID: 8887053
21. Dib-Hajj SD, Yang Y, Waxman SG (2008) Genetics and molecular pathophysiology of Na(v)1.7-related pain syndromes. Adv Genet 63: 85–110. doi:10.1016/S0065-2660(08)01004-3, PMID: 19185186
22. Duan K-Z, Xu Q, Zhang X-M et al (2012) Targeting A-type K(+) channels in primary sensory neurons for bone cancer pain in a rat model. Pain 153:562–574. doi:10.1016/j.pain.2011.11.020, PMID: 22188869
23. Everill B, Kocsis JD (1999) Reduction in potassium currents in identified cutaneous afferent dorsal root ganglion neurons after axotomy. J Neurophysiol 82:700–708, PMID: 10444667
24. Fan N, Donnelly DF, LaMotte RH (2011) Chronic compression of mouse dorsal root ganglion alters voltage-gated sodium and potassium currents in medium-sized dorsal root ganglion neurons. J Neurophysiol 106:3067–3072. doi:10.1152/jn.00752.2011, PMID: 21917996
25. Fan N, Sikand P, Donnelly DF et al (2011) Increased Na^+ and K^+ currents in small mouse dorsal root ganglion neurons after ganglion compression. J Neurophysiol 106:211–218. doi:10.1152/jn.00065.2011, PMID: 21525373
26. Feng B, Strichartz G (2009) Endothelin-1 raises excitability and reduces potassium currents in sensory neurons. Brain Res Bull 79: 345–350. doi:10.1016/j.brainresbull.2009.04.012, PMID: 19409452
27. Gardiner NJ, Cafferty WBJ, Slack SE, Thompson SWN (2002) Expression of gp130 and leukaemia inhibitory factor receptor subunits in adult rat sensory neurones: regulation by nerve injury. J Neurochem 83:100–109, PMID: 12358733
28. Gilchrist J, Bosmans F (2012) Animal toxins can alter the function of Nav1.8 and Nav1.9. Toxins (Basel) 4:620–632. doi:10.3390/toxins4080620, PMID: 23012651
29. Gutman GA, Chandy KG, Grissmer S et al (2005) International Union of Pharmacology. LIII. Nomenclature and molecular relationships of voltage-gated potassium channels. Pharmacol Rev 57:473–508. doi:10.1124/pr.57.4.10, PMID: 16382104
30. Heinrich PC, Behrmann I, Müller-Newen G et al (1998) Interleukin-6-type cytokine signalling through the gp130/Jak/STAT pathway. Biochem J 334(Pt 2):297–314, PMID: 9716487
31. Heinrich PC, Behrmann I, Haan S et al (2003) Principles of interleukin (IL)-6-type cytokine signalling and its regulation. Biochem J 374: 1–20. doi:10.1042/BJ20030407, PMID: 12773095
32. Hirano T (1998) Interleukin 6 and its receptor: ten years later. Int Rev Immunol 16:249–284. doi:10.3109/08830189809042997, PMID: 9505191
33. Iftinca MC, Zamponi GW (2009) Regulation of neuronal T-type calcium channels. Trends Pharmacol Sci 30:32–40. doi:10.1016/j.tips.2008.10.004, PMID: 19042038
34. Ishikawa K, Tanaka M, Black JA, Waxman SG (1999) Changes in expression of voltage-gated potassium channels in dorsal root ganglion neurons following axotomy. Muscle Nerve 22:502–507, PMID: 10204786
35. Jagodic MM, Pathirathna S, Joksovic PM et al (2008) Upregulation of the T-type calcium current in small rat sensory neurons after chronic constrictive injury of the sciatic nerve. J Neurophysiol 99: 3151–3156. doi:10.1152/jn.01031.2007, PMID: 18417624
36. Jentsch TJ (2000) Neuronal KCNQ potassium channels: physiology and role in disease. Nat Rev Neurosci 1:21–30. doi:10.1038/35036198, PMID: 11252765
37. Johnston J, Forsythe ID, Kopp-Scheinpflug C (2010) Going native: voltage-gated potassium channels controlling neuronal excitability. J Physiol 588:3187–3200. doi:10.1113/jphysiol.2010.191973, PMID: 20519310
38. Kiefer R, Kieseier BC, Stoll G, Hartung HP (2001) The role of macrophages in immune-mediated damage to the peripheral nervous system. Prog Neurobiol 64:109–127, PMID: 11240209
39. Koerber HR, Druzinsky RE, Mendell LM (1988) Properties of somata of spinal dorsal root ganglion cells differ according to peripheral receptor innervated. J Neurophysiol 60:1584–1596, PMID: 3199173
40. Kostyuk PG, Veselovsky NS, Fedulova SA, Tsyndrenko AY (1981) Ionic currents in the somatic membrane of rat dorsal root ganglion neurons-III Potassium currents. Neuroscience 6:2439–2444, PMID: 6275296
41. Lampert A, Hains BC, Waxman SG (2006) Upregulation of persistent and ramp sodium current in dorsal horn neurons after spinal cord injury. Exp Brain Res 174:660–666. doi:10.1007/s00221-006-0511-x, PMID: 16718433
42. Lampert A, O'Reilly AO, Reeh P, Leffler A (2010) Sodium channelopathies and pain. Pflugers Arch 460:249–263. doi:10.1007/s00424-009-0779-3, PMID: 20101409
43. Langeslag M, Constantin CE, Andratsch M et al (2011) Oncostatin M induces heat hypersensitivity by gp130-dependent sensitization of TRPV1 in sensory neurons. Mol Pain 7:102. doi:10.1186/1744-8069-7-102, PMID: 22196363
44. Lawson SN (2002) Phenotype and function of somatic primary afferent nociceptive neurones with C-, Adelta- or Aalpha/beta-fibres. Exp Physiol 87:239–244, PMID: 11856969
45. Liu M, Wood JN (2011) The roles of sodium channels in nociception: implications for mechanisms of neuropathic pain. Pain Med 12(Suppl 3):S93–S99. doi:10.1111/j.1526-4637.2011.01158.x, PMID: 21752183
46. Lumpkin EA, Marshall KL, Nelson AM (2010) The cell biology of touch. J Cell Biol 191:237–248. doi:10.1083/jcb.201006074, PMID: 20956378
47. Matsuyoshi H, Takimoto K, Yunoki T et al (2012) Distinct cellular distributions of Kv4 pore-forming and auxiliary subunits in rat dorsal root ganglion neurons. Life Sci 91:258–263. doi:10.1016/j.lfs.2012.07.007, PMID: 22820170
48. Murphy PG, Ramer MS, Borthwick L et al (1999) Endogenous interleukin-6 contributes to hypersensitivity to cutaneous stimuli and changes in neuropeptides associated with chronic nerve constriction in mice. Eur J Neurosci 11:2243–2253, PMID: 10383613
49. Novakovic SD, Tzoumaka E, McGivern JG et al (1998) Distribution of the tetrodotoxin-resistant sodium channel PN3 in rat sensory neurons in normal and neuropathic conditions. J Neurosci 18:2174–2187, PMID: 9482802
50. Obreja O, Rathee PK, Lips KS et al (2002) IL-1 beta potentiates heat-activated currents in rat sensory neurons: involvement of IL-1RI, tyrosine kinase, and protein kinase C. FASEB J 16:1497–1503. doi:10.1096/fj.02-0101com, PMID: 12374772
51. Okubo K, Matsumura M, Kawaishi Y et al (2012) Hydrogen sulfide-induced mechanical hyperalgesia and allodynia require activation of both Cav3.2 and TRPA1 channels in mice. Br J Pharmacol 166: 1738–1743. doi:10.1111/j.1476-5381.2012.01886.x, PMID: 22300342
52. Passmore G, Delmas P (2011) Does cure for pain REST on Kv7 channels? Pain 152:709–710. doi:10.1016/j.pain.2011.02.040, PMID: 21377798
53. Phuket TRN, Covarrubias M (2009) Kv4 Channels Underlie the Subthreshold-Operating A-type K-current in Nociceptive Dorsal Root Ganglion Neurons. Front Mol Neurosci 2:3. doi:10.3389/neuro.02.003.2009, PMID: 19668710
54. Quarta S, Vogl C, Constantin CE et al (2011) Genetic evidence for an essential role of neuronally expressed IL-6 signal transducer gp130 in the induction and maintenance of experimentally induced mechanical hypersensitivity in vivo and in vitro. Mol Pain 7:73. doi:10.1186/1744-8069-7-73, PMID: 21951917
55. Rasband MN, Park EW, Vanderah TW et al (2001) Distinct potassium channels on pain-sensing neurons. Proc Natl Acad Sci U S A 98: 13373–13378. doi:10.1073/pnas.231376298, PMID: 11698689

56. Renganathan M, Cummins TR, Waxman SG (2001) Contribution of Na(v)1.8 sodium channels to action potential electrogenesis in DRG neurons. J Neurophysiol 86:629–640, PMID: 11495938
57. Richards PJ, Nowell MA, Horiuchi S et al (2006) Functional characterization of a soluble gp130 isoform and its therapeutic capacity in an experimental model of inflammatory arthritis. Arthritis Rheum 54: 1662–1672. doi:10.1002/art.21818, PMID: 16646038
58. Sarria I, Ling J, Gu JG (2012) Thermal sensitivity of voltage-gated Na^+ channels and A-type K^+ channels contributes to somatosensory neuron excitability at cooling temperatures. J Neurochem 122:1145–1154. doi:10.1111/j.1471-4159.2012.07839.x, PMID: 22712529
59. Scholfield CN (1990) Properties of K-currents in unmyelinated presynaptic axons of brain revealed revealed by extracellular polarisation. Brain Res 507:121–128, PMID: 1689201
60. Smith PC, Hobisch A, Lin DL et al (2001) Interleukin-6 and prostate cancer progression. Cytokine Growth Factor Rev 12:33–40, PMID: 11312117
61. Takeda M, Tsuboi Y, Kitagawa J et al (2011) Potassium channels as a potential therapeutic target for trigeminal neuropathic and inflammatory pain. Mol Pain 7:5. doi:10.1186/1744-8069-7-5, PMID: 21219657
62. Tappe-Theodor A, Constantin CE, Tegeder I et al (2012) Gα(q/11) signaling tonically modulates nociceptor function and contributes to activity-dependent sensitization. Pain 153:184–196. doi:10.1016/j.pain.2011.10.014, PMID: 22071319
63. Todorovic SM, Jevtovic-Todorovic V (2011) T-type voltage-gated calcium channels as targets for the development of novel pain therapies. Br J Pharmacol 163:484–495. doi:10.1111/j.1476-5381.2011.01256.x, PMID: 21306582
64. Uchida H, Sasaki K, Ma L, Ueda H (2010) Neuron-restrictive silencer factor causes epigenetic silencing of Kv4.3 gene after peripheral nerve injury. Neuroscience 166:1–4. doi:10.1016/j.neuroscience.2009.12.021, PMID: 20006971
65. Winkelman DLB, Beck CL, Ypey DL, O'Leary ME (2005) Inhibition of the A-type K^+ channels of dorsal root ganglion neurons by the long-duration anesthetic butamben. J Pharmacol Exp Ther 314:1177–1186. doi:10.1124/jpet.105.087759, PMID: 15923341
66. Yang E-K, Takimoto K, Hayashi Y et al (2004) Altered expression of potassium channel subunit mRNA and α-dendrotoxin sensitivity of potassium currents in rat dorsal root ganglion neurons after axotomy. Neuroscience 123:867–874. doi:10.1016/j.neuroscience.2003.11.014
67. Zhao X, Tang Z, Zhang H et al (2013) A long noncoding RNA contributes to neuropathic pain by silencing Kcna2 in primary afferent neurons. Nat Neurosci 16:1024–1031. doi:10.1038/nn.3438, PMID: 23792947
68. Zhu W, Oxford GS (2011) Differential gene expression of neonatal and adult DRG neurons correlates with the differential sensitization of TRPV1 responses to nerve growth factor. Neurosci Lett 500:192–196. doi:10.1016/j.neulet.2011.06.034, PMID: 21741445